The reconstruction of dipolar surfaces: a preliminary step for adsorption modeling

The reconstruction of dipolar surfaces: a preliminary step for adsorption modelling

M. Bruno

Dipartimento di Scienze della Terra, Università degli Studi di Torino, Via Valperga Caluso 35, 10125, Torino, Italy

Key words dipolar surfaces, reconstruction, surface energy

In this brief review the crystal dipolar surfaces and the way to stabilize them are discussed. Two classes of crystals are interested: intrinsically polar crystals and non-polar crystals, where the polarity along some directions is the consequence of the alternating layers of positive and negative charges. I discuss the importance of taking into account the bulk symmetry of the crystal when a surface reconstruction is performed. As examples, different reconstructions of the {111} form of halite (NaCl), and the {01.2} and {00.1} forms of calcite ($CaCO_3$) are discussed in detail.

1 Introduction

The real surface profile of a (*hkl*) face rarely coincides with the ideal *hkl* lattice plane. In other words, the *hkl* plane is a geometrical abstraction of the crystal structure, while to generate the corresponding surface profile, one has to consider the face character: flat (F), stepped (S) or kinked (K), according to the Hartman-Perdok theory [1-4], along with its interactions with the mother phase. Calculation shows that stability problems can arise, owing to the surface polarity, either in polar crystals (not center-symmetric crystals) or on peculiar faces of non-polar crystals, since the infinite 2D array of iso-oriented surface dipole moments makes infinite the value of the electrical field in the surface sites. Two classes of crystals are interested: intrinsically polar crystals, such as ZnS–wurtzite like ($P6_3mc$) or ZnS–sphalerite like ($F\bar{4}3m$) lattices, and those, non-polar, where the polarity along some directions (directions with a macroscopic dipole are often called *dipolar directions*) is the consequence of the alternating layers of positive and negative charges (such as the {111} form of the NaCl–like lattice).

When simulating the interfacial properties for ionic crystals it is often convenient to consider the crystal structure as a stack of planes. If the stack consists of charged planes, the electrostatics may be ill-conditioned. For example, the [111] direction of the rock-salt structure and the [100] direction of the fluorite structure define a stack of alternating, equally spaced planes of opposite sign. This gives a dipole moment normal to the surface that is proportional to the number of pairs of planes in the stack. It does not occur for all stacks of charged planes; for example, the [111] direction of the fluorite structure defines a stack of charged planes, but there is no macroscopic dipole. Any attempt to form a surface by breaking such a stack will fail because the electrostatic energy diverges. Such surfaces can only exist if they are stabilised by defects. This is the basis of the classification of surfaces grounded on the Tasker's rules [5] which identified three types of surfaces in ionic or partly ionic crystal, which are schematized in Fig. 1. Type I consists of neutral planes with both anions and cations (Fig. 1a). Type II consists of charged planes arranged symmetrically so that there is no dipole moment perpendicular to the unit cell (Fig. 1b). The type III surface is charged and there is a perpendicular dipole moment. These surfaces have infinite surface energies (or very large surface energies for finite crystals) and produce a polarising electric field in the bulk. An electrostatic argument therefore indicates that such surfaces cannot exist.

Examples of such surface typologies are reported in Fig. 1. In Fig. 1d the (100) and (110) faces of binary ionic crystals, with general formula MX, including most of the alkali halides (e. g. NaCl) and many metal oxides (e.g. MgO, NiO), are reported. These surfaces are both neutral and type I. Instead, in Fig. 1e the (111) face of ionic crystals of the type MX_2 with fluorite structure, including

alkaline-earth halides and oxides such as UO_2 and ThO_2, is reported; this surface is neutral and of type II. Finally, in Fig. 1f the (111) face of MX ionic crystals is drawn, which is charged and of Type III.

To explain the presence of unstable surfaces of Type III, either at equilibrium or during growth, one has to invoke (i) modifications at the atomic level induced by adsorption of foreign substances and/or (ii) a reconstruction of the surfaces to cancel out the 2D-dipole arrays, and/or, as it was suggested for some forms of covalent phases [6,7], (iii) a rearrangement of the electronic structure resulting in an effective charge transfer between the polar surfaces. In any case, a criterion for surface reconstruction or for its electronic rearrangement is needed, also when dealing with foreign adsorption.

The reconstruction is performed by modifying the density of ions in the outermost layers of the crystal by the introduction of vacancies. Usually, this is done by moving charge from the outer planes of the stack to form new planes at the bottom. In practice, the macroscopic dipole moment is quenched by modifying the ionic density (or charge density) on the *m* outer planes according to the relation [8]:

$$\sum_{j=1}^{m} \sigma_j = -(\sigma_{m+1}/2) \qquad (1)$$

where σ_j is the charge density of the *j*-th plane.

Reconstructions usually found in literature consist in removing 50% of the atoms from the outmost *hkl* layer and in relocating them on its centre-symmetrical $\bar{h}\bar{k}\bar{l}$ plane, regardless of the topology obtained by the atoms removal. Actually, this reconstruction which fulfils both condition of electro-neutrality and dipole annihilation on the surface, is not self-consistent owing to a serious drawback when dealing with the search for the minimum of the specific free energy (γ_{hkl}) of the reconstructed surfaces. As a matter of fact, there are many ways to remove one half surface ions and to each is associated a value of γ_{hkl}.

In the following, we will show the importance of taking into account the bulk symmetry of the crystal when a surface reconstruction is performed. Different reconstructions of the {111} form of halite, and the {01.2} and {00.1} forms of calcite are discussed in detail. But before to deal with such examples, the reasons why the electrostatic potential and the surface energy diverge, for a polar face, are explained.

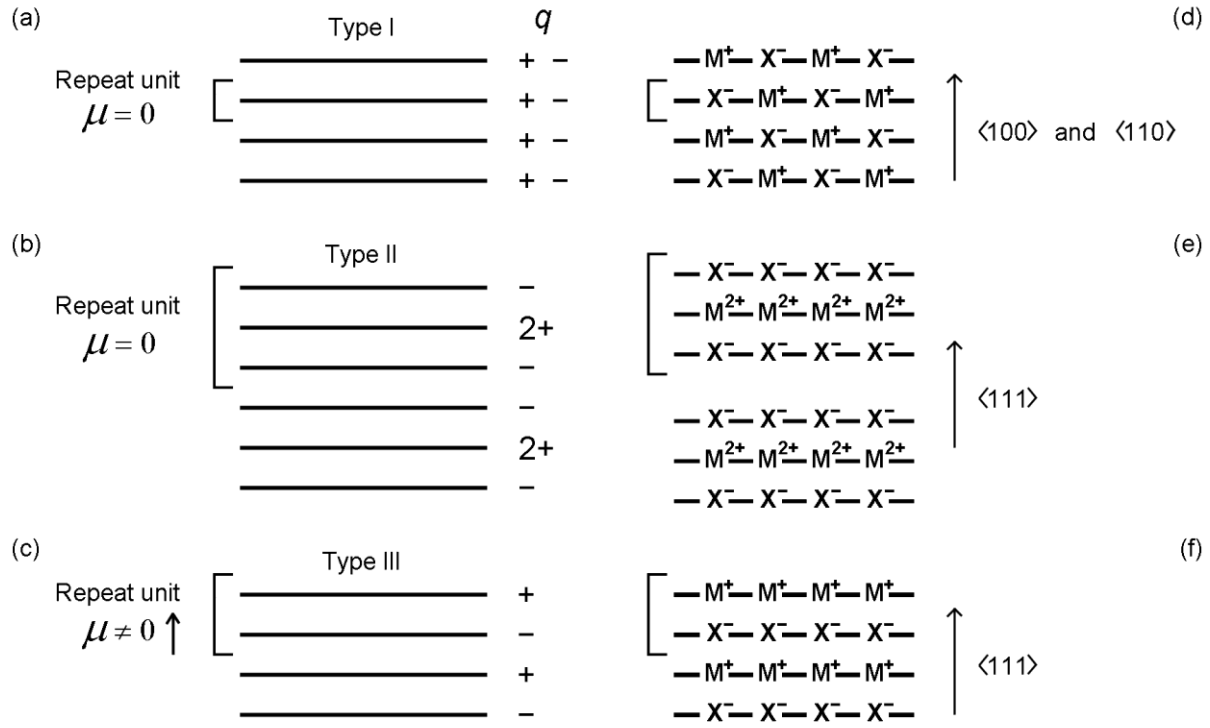

Fig. 1 Surfaces classification according to Tasker [5]: (a) and (d) Type I, each plane contains an equal number of cations and anions (the net dipole moment is zero; $\mu = 0$); (b) and (e) Type II, each plane is charged, but the there is not a net dipole moment perpendicular to the surface ($\mu = 0$); (c) and (f) Type III, charged planes and dipole moment normal to the surface ($\mu \neq 0$). Redrawn from ref [5].

2 Why does the surface energy diverges for a polar slab?

Let us consider a polar slice consisting of two parallel planes, separated by a distance l and having the same, but opposite charge density σ (Fig. 2). Furthermore, let us suppose that the polar slices are stacked one upon the other with a repeat distance d. The electrostatic potential V_m in a point P with respect to the m-th polar slice is then evaluated as follow. Consider in each plane a disc with radius r, the centre of which lies perpendicularly under P. The potential V_m is then:

$$V_m = \int_0^r \frac{2\pi r\sigma dr}{\sqrt{r^2 + (md)^2}} - \int_0^r \frac{2\pi r\sigma dr}{\sqrt{r^2 + (md + l)^2}} \tag{2}$$

After integration and development of the obtained square roots in a series, one finds:

$$V_m = 2\pi\sigma l\left(1-\frac{2md+l}{2\sqrt{r^2+(md)^2}}+...\right) \tag{3}$$

By considering $r\to\infty$ and a certain value of *m*, $V_m = 2\pi\sigma l$; the two-planes repeat unit produces a potential at large distances. Then, the potential generated by *n* polar slices is:

$$V=\sum_{m=1}^{n}V_m=\sum_{m=1}^{n}2\pi\sigma l = n2\pi\sigma l \tag{4}$$

Therefore, when there is a dipole moment perpendicular to the surface of an infinite crystal, $n\to\infty$, the potential (4) diverges, $V\to\infty$. A more detailed discussion on the Eqs. (2)-(4) is reported in the paper by Hartman [9].

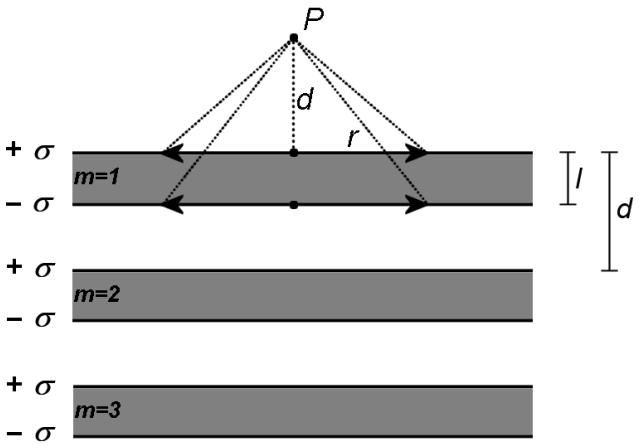

Fig. 2 A schematic representation of a polar face composed by a stack of polar slice (with a repeat distance *d*) consisting of two parallel planes, separated by a distance *l* and having the same, but opposite charge density σ. Redrawn from ref [9].

Now, we want to calculate the electrostatic contribution to the surface energy. For doing this we imagine an infinite crystal divided into two halves by a surface plane. The surface energy is the energy of cohesion between the two halves of the crystal, which may be obtained by summing, over each ion in one half of the crystal, the product of its charge and the potential due to ions in the other half. Then, for the surface energy we have:

$$\gamma = \frac{1}{A}\sum_i q_i V(\mathbf{r}_i) \tag{5}$$

where q_i is the charge of the *i*-th ion in one half of the crystal, $V(\mathbf{r}_i)$ is the electrostatic potential generated by the ions in the other half of the crystal at $\mathbf{r}_i$, the position vector of the *i*-th ion, and *A* is the area of the surface unit cell. By considering the relation (4), we observe that $\gamma \to \infty$ when a crystal having infinite thickness ($n \to \infty$) is considered.

3 The {111} form of halite

The halite (NaCl) crystal is cubic with space group *Fm3m* and $Z = 4$ (four formula units per cell); the lattice parameter is $a = 5.6401(2)$ Å at room temperature.

The NaCl crystals obtained from vapour growth show exclusively the {100} form. The morphology of NaCl crystals grown from aqueous solution results to be richer. In fact, in that case they show {110} and {111} forms when a given amount of specific impurity (*e.g.*, urea, formamide, $CdCl_2$) is added to the growth medium [10,11], even if {111} NaCl faces can also be obtained from pure water solution [10,12]. It was observed that if NaCl like crystals grow at low supersaturation only cubic crystals were formed, while, at higher supersaturations, well developed {111} faces appear.

In the past, to explain the presence of the {111} form in ionic crystals with rocksalt-type structures grown from aqueous solution, the adsorption of impurities, H_2O molecules and/or H^+ and OH^- ions was invoked [13,14]. Instead, when no impurities are present, theoretical calculation suggests two possibilities to stabilize the {111} surfaces: (a) the bulk terminated {111} surfaces break up into neutral {100} facets upon annealing [14] or (b) the surfaces reconstruct. In our case, by applying the relation (1) to the (111) slab we can obtain two surface reconstructions. The first one is performed by only modifying the outer plane (*e.g.*, the plane containing the Na ions) of the slab: one half of Na ions must be moved from the outer plane of the (111) slab to a new plane at the bottom to produce a slab that is symmetrical about a central plane. In this way, the charge density of the latter plane (σ_1) equals half of the charge density of the second crystal plane $(\sigma_1 = -\sigma_2/2)$. The same procedure is also valid when the outer plane of the slab is composed by Cl ions. The second type of surface reconstruction (octopolar reconstruction; Figure 3), was firstly proposed by Hartman [15] and later on by Lacmann [16] who postulated that all the NaCl surfaces should be reconstructed in such a way that the finite crystal only terminates with complete $(NaCl)_4$ molecules (octopoles). It is performed by removing the 75% of ions in the outer layer of the slab and the 25% of ions in the underneath one; then, $\sigma_1 = \sigma_3/4$ and $\sigma_2 = -3\sigma_3/4$. As in the previous case, the octopolar (111) surfaces may be either Na or Cl terminated. In the following we will refer to these

two surface reconstructions as R1 and R2 ones, respectively; we will use henceforth the notation $(111)_A^B$, where *A* = R1 or R2, and *B* = Na or Cl, to indicate the different surface reconstructions and terminations.

Both of these reconstructions generate an electrically neutral slab, but only the {111} octopolar reconstructed surfaces respect the symmetry of the point group of the surface, being preserved the three-fold axis perpendicular to the 111 plane. Wolf [17] confirmed this "octopole" reconstruction hypothesis, which cancels the divergence of the electric field at the {111} crystal surfaces, by calculations of the (111) NaCl surface energy in contact with vacuum. Nevertheless, reconstructed octopolar {111} surfaces were never observed in NaCl crystals, neither at equilibrium nor during growth from the vapour phase.

Bruno et al. [18,19] obtained detailed information on the structure of the (100), (110), $(111)_{R1}^{Na}$, $(111)_{R1}^{Cl}$, $(111)_{R2}^{Na}$ and $(111)_{R2}^{Cl}$ surfaces of NaCl crystals. They performed a quantum mechanical study of the structure of the (100), (110), $(111)_{R1}^{Na}$, $(111)_{R1}^{Cl}$, $(111)_{R2}^{Na}$ and $(111)_{R2}^{Cl}$ surfaces, whose geometries were optimized at DFT level (B3LYP Hamiltonian). Furthermore, in order to verify if the R1 reconstructed (111) face is more stable than the R2 reconstructed one, the surface energies at *T* = 0 K of the (100), (110), $(111)_{R1}^{Na}$, $(111)_{R1}^{Cl}$, $(111)_{R2}^{Na}$ and $(111)_{R2}^{Cl}$ surfaces were determined. The calculations (geometry optimization and surface energy) were performed with the CRYSTAL06 program [20] and by considering a 2D slab model. Each slab of given thickness was generated by cutting the ideal bulk structure parallel to the face of interest [(100), (110) and (111)], and by eliminating the atoms in excess, in the case of (111) face, in order to perform the R1 and R2 reconstructions. Details on the computational parameters and the relaxed surface structures are reported in Bruno et al. [18,19].

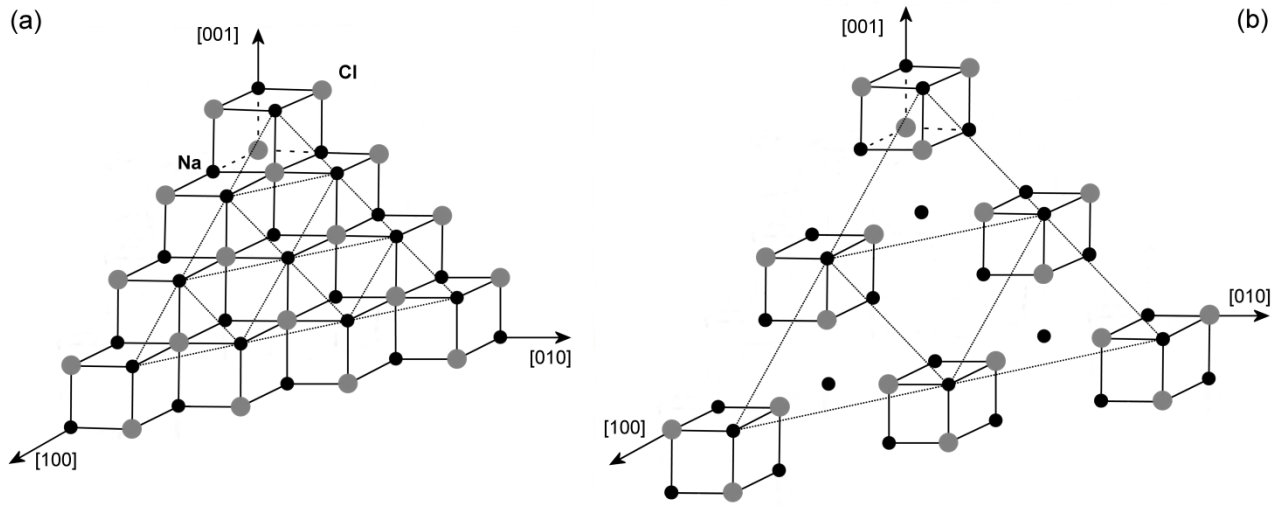

Fig. 3 The unreconstructed (a) and reconstructed (b) (111) Na-terminated surfaces of NaCl are redrawn from ref [18]. The reconstructed $(111)^{Na}$ face is made up by $(NaCl)_4$ molecules (octopoles): the outermost layer of the $(111)^{Na}$ surface contains only 1/4 of the available lattice sites, while the two layers below contain 3/4 and 4/4 of the sites, respectively. *Dotted lines* join the atoms belonging to the outermost layer.

The surface energy at 0 K [$\gamma(0)$] has been calculated using the relation [21]:

$$\gamma(0) = \lim_{n\to\infty} E_s(n) = \lim_{n\to\infty} \frac{E(n) - n\left[E(n) - E(n-1)\right]}{2A} \tag{6}$$

where *A* is the area of the primitive unit cell of the surface, and *E(n)* is the energy of a *n*-layer slab; the factor 2 in the denominator accounts for the upper and lower surfaces of the slab. $E_s(n)$ is thus the energy per unit area required to form the surface from the bulk. As more layers are added in the calculation $(n \to \infty)$, $E_s(n)$ will converge to the surface energy per unit area, $\gamma(0)$; the slab thicknesses considered were sufficient to reach convergence of the γ values.

The resulting values of the relaxed (γ^r) and unrelaxed (γ^u) surface energies at T = 0 K are reported in Table 1. The stability order of the relaxed surfaces is $(100) < (110) < (111)^{Cl}_{R2} < (111)^{Na}_{R2} < (111)^{Na}_{R1} < (111)^{Cl}_{R1}$. It is worth noting that in the case of the R1 reconstruction the Na-terminated surface is more stable than the Cl-terminated one, whereas for the R2 reconstruction the opposite is true. Instead, the relative stability order of the unrelaxed surfaces is $(100) < (110) < (111)^{Na}_{R2} = (111)^{Cl}_{R2} < (111)^{Cl}_{R1} < (111)^{Na}_{R1}$. According to these calculations, the octopolar reconstruction (R2) is favoured with respect to the R1 reconstruction for both the relaxed and unrelaxed surfaces.

Table 1 Relaxed, γ^r, and unrelaxed, γ^u, surface energies at 0K of the (100), (110), $(111)^{Na}_{R1}$, $(111)^{Cl}_{R1}$, $(111)^{Na}_{R2}$ and $(111)^{Cl}_{R2}$ faces of NaCl [18,19].

	(100)	(110)	$(111)^{Na}_{R1}$	$(111)^{Cl}_{R1}$	$(111)^{Na}_{R2}$	$(111)^{Cl}_{R2}$
γ^r (J/m^2)	0.160	0.330	0.520	0.530	0.405	0.390
γ^u (J/m^2)	0.161	0.387	0.825	0.769	0.551	0.552

4 The {01.2} form of calcite

Calcite [rhombohedral, space group $R\bar{3}c$, with two formula units (Z) per cell, but often described in a hexagonal cell having Z = 6] is the stable polymorph of $CaCO_3$ at room temperature and pressure. Its structure consists of an alternate stacking of planar CO_3 groups and Ca ions along the *c* axis of the hexagonal cell.

According to the Hartman-Perdok theory [1-4], the {01.2} rhombohedron is a flat form [22]: two PBCs run within a slice $d_{01.2} = 3.85$ Å thick, along the $\langle 42\bar{1} \rangle$ and $\langle 010 \rangle$ directions. If observed along the [100] direction, the (01.2) face is composed of alternating layers of Ca ions and CO_3 groups: hence, such a face is a dipolar one (Fig. 4). Therefore, in order to quench the macroscopic dipole moment, it is necessary to reconstruct the surface.

By applying the relation (1) to the (01.2) slab and supposing that the outer plane only is modified (e.g., the plane of the Ca ions), the charge density of the latter plane (σ_1) equals half of the charge density of the second crystal plane $(\sigma_1 = -\sigma_2/2)$. Then, in order to delete the macroscopic dipole moment, one half of Ca ions must be moved from the outer plane of the (01.2) slab to a new plane at the bottom to produce a slab that is symmetrical about a central plane; the same procedure applies when the outer plane of the slab is composed by CO_3 groups. The coverage degree, θ_{Ca} or θ_{CO3}, resulting from this type of reconstruction is 0.5.

Recently, by respecting the electroneutrality constraint as explained above, and by applying the Hartman-Perdok constraints on the dipole moment of the PBCs, Massaro et al. [23] identified two type of reconstructions that could be performed on the (01.2) face: (i) R2 reconstruction: the outermost layer is based on the $[010] \times 1/3[211]$ rectangular mesh, which is symmetrical with respect to the *c* glide plane of the crystal, thus fulfilling the 2D symmetry of the face; (ii) R1 reconstruction: the outermost layer is based on a $1/6[42\bar{1}] \times 1/6[2\bar{2}1]$ lozenge shaped mesh that does not respect the 2D symmetry of the face. In the following, since both of these reconstructions can be either Ca or CO_3 terminated, we will use the notation $(01.2)^B_A$, where *A* = R1 or R2, and *B* = Ca or CO_3, to indicate the assumed different surface reconstructions and terminations.

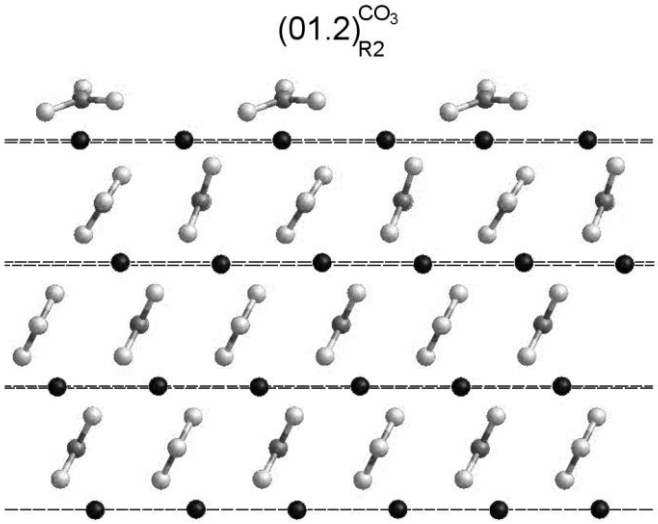

Fig. 4 Relaxed structure of the $(01.2)^{CO_3}_{R2}$ slab, redrawn from ref [24]. The slabs is viewed along the [100] direction.

Bruno et al. [24] obtained detailed information on the structure of the $(01.2)^{Ca}_{R1}$, $(01.2)^{CO_3}_{R1}$, $(01.2)^{Ca}_{R2}$ and $(01.2)^{CO_3}_{R2}$ surfaces. At the empirical level, the slab geometries were optimized by using the inter-atomic potential for calcite developed by Rohl et al. [25] and the GULP simulation code [26]. In addition, searching for a relationship between the results we obtained and the calculation method we employed, the structures of the $(01.2)^{Ca}_{R1}$ and $(01.2)^{CO_3}_{R1}$ slabs were also optimized from first principles, at the DFT level (B3LYP Hamiltonian) with the CRYSTAL06 code. Furthermore, the surface energies of the $(01.2)^{Ca}_{R1}$, $(01.2)^{CO_3}_{R1}$, $(01.2)^{Ca}_{R2}$ and $(01.2)^{CO_3}_{R2}$ faces were determined (Table 2). Details on the computational parameters and the relaxed surface structures are reported in Bruno et al. [24].

The relaxed surface energies determined with both GULP and CRYSTAL06 are in excellent agreement. The stability order of the relaxed faces is $(01.2)^{CO_3}_{R2} < (01.2)^{Ca}_{R1} < (01.2)^{CO_3}_{R1} < (01.2)^{Ca}_{R2}$, whereas the stability order of the unrelaxed ones is $(01.2)^{Ca}_{R2} < (01.2)^{Ca}_{R1} < (01.2)^{CO_3}_{R2} < (01.2)^{CO_3}_{R1}$. As in the case of the (111) NaCl face, the R2 reconstruction (the most symmetric one) is favoured with respect to the R1 reconstruction for both the relaxed and unrelaxed surfaces.

Table 2 Relaxed, γ^r, and unrelaxed, γ^u, surface energies at 0K of the $(01.2)^{Ca}_{R1}$, $(01.2)^{CO_3}_{R1}$, $(01.2)^{Ca}_{R2}$ and $(01.2)^{CO_3}_{R2}$ faces of calcite [24].

$(01.2)^{Ca}_{R1}$	$(01.2)^{CO_3}_{R1}$	$(01.2)^{Ca}_{R2}$	$(01.2)^{CO_3}_{R2}$

γ^r (J/m^2)	0.953	0.982	1.040	0.750	GULP
γ^u (J/m^2)	3.402	3.791	2.719	3.661	

γ^r (J/m^2)			1.060	0.750	CRYSTAL
γ^u (J/m^2)			2.050		

5 The {00.1} form of calcite

In this section we deal with the reconstruction of the {00.1} form of calcite. According to Hartman-Perdok [1-4], {00.1} is a kinked form (K character). Further, it shows surface polarity since its surface is made of alternating layers of Ca ions and CO_3 groups, as it comes out when the structure is observed along any direction perpendicular to the [001] triad axis.

The calcite structure, when viewed perpendicularly to its three-fold [001] axis, is very similar to that of rock-salt structure projected perpendicularly to the <111> directions. Indeed, it can be simply imagined as a replacement of the Na cations by Ca and of the Cl anions by CO_3 groups, coupled with a compression along the [001] axis (Fig. 5). Hence, both R1 and R2 reconstructions already employed for the {111} NaCl surface, can also be considered for stabilizing the {00.1} surface of calcite. Moreover, both reconstructions being either Ca or CO_3 terminated, we will use the notation $(00.1)^B_A$, where A = R1 or R2, and B = Ca or CO_3, to distinguish among the different surface reconstructions and terminations.

In order to determine which one of the reconstructions is favoured, the surface energies related to the four $(00.1)^{Ca}_{R1}$, $(00.1)^{CO_3}_{R1}$, $(00.1)^{Ca}_{R2}$ and $(00.1)^{CO_3}_{R2}$ profiles were calculated [27], before and after surface relaxation. Calculations (slab geometries optimizations and surface energy estimates) were only performed by using the inter-atomic potential for calcite developed by Rohl et al. [25] and the GULP simulation code [26].

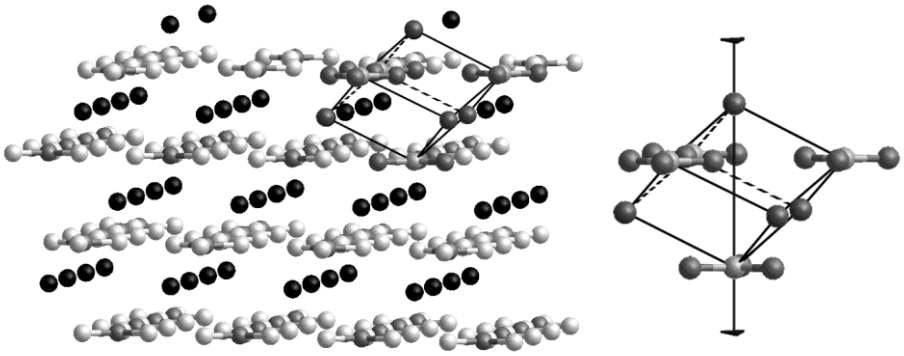

Fig. 5 Octopolar reconstruction of the Ca terminated (00.1) face of calcite, which is performed by removing the 75% of the Ca ions in the outer layer and 25% of the CO_3 groups in the underneath one. The calcite octopole, composed by four Ca ions and four CO_3 groups stacked along the three-fold axis, is also reported. Redrawn from ref [27].

The resulting values of the surface energies at 0K are reported in Table 3. The stability order of the relaxed faces is $(00.1)^{CO_3}_{R2} < (00.1)^{CO_3}_{R1} < (00.1)^{Ca}_{R1} < (00.1)^{Ca}_{R2}$, whereas the stability order of the unrelaxed ones is $(00.1)^{CO_3}_{R2} = (00.1)^{Ca}_{R2} < (00.1)^{CO_3}_{R1} < (00.1)^{Ca}_{R1}$. Also in this case the R2 reconstruction results to be favoured with respect to the R1 reconstruction for both the relaxed and unrelaxed surfaces.

Table 3. Relaxed, γ^r, and unrelaxed, γ^u, surface energies at 0K of the $(00.1)^{Ca}_{R1}$, $(00.1)^{CO_3}_{R1}$, $(00.1)^{Ca}_{R2}$ and $(00.1)^{CO_3}_{R2}$ faces of calcite [27].

	$(00.1)^{Ca}_{R1}$	$(00.1)^{CO_3}_{R1}$	$(00.1)^{Ca}_{R2}$	$(00.1)^{CO_3}_{R2}$
γ^r (J/m^2)	0.834	0.764	0.849	0.711
γ^u (J/m^2)	2.476	1.720	1.654	1.654

6 Conclusions

(i) Among all the reconstructed surfaces the most stable one resulted to be that respecting the bulk symmetry of the crystal. As a matter of fact, the “octopolar reconstruction” is favoured with respect to all the other ones when dealing with a face ruled by a three-fold symmetry.

(ii) We can state that the bulk crystal symmetry has to be necessarily considered to achieve the self consistency of the surface reconstruction: the symmetry group of a reconstructed surface must be a subgroup of the symmetry of the bulk crystal viewed along the normal to the surface. We can also express these considerations by means of the Curie's symmetry principle [28], which may be formulated for the crystal surfaces as follows:

the symmetry group of a crystal face in its mother phase is given by the maximal common subgroup of the symmetry group of the bulk crystal and of the symmetry group of the mother phase.

For the crystal/vacuum system, only the symmetry group of the crystal bulk can impose constraints on the symmetry group of the face. Then, according to the Curie's principle the face should have the maximal subgroup of the symmetry of the crystal bulk projected along the normal to the surface.

(iii) The determination of the most probable surface symmetry is of fundamental importance to gain more insights on impurities adsorption, epitaxy and twinning. Indeed, the modelling and interpretation of such phenomena require the knowledge of the structure of the interface on which the phenomenon occurs. Then, we think that the considerations on the surface symmetry reported in this work can give a useful contribution to the understanding of the interfacial processes.

References

[1] P. Hartman, Crystal Growth: An Introduction, Hartman P. (Ed.), North-Holland, Amsterdam, 1973, p. 367.

[2] P. Hartman and W. G. Perdok, Acta Cryst. **8**, 49 (1955).

[3] P. Hartman and W. G. Perdok, Acta Cryst. **8**, 521 (1955).

[4] P. Hartman and W. G. Perdok, Acta Cryst. **8**, 525 (1955).

[5] P. W. Tasker, J. Phys. C: Solid State Phys. **12**, 4977 (1979).

[6] A. Pojani, F. Finocchi and C. Noguera, Appl. Surf. Sci. **142**, 177 (1999).

[7] A. Wander, F. Schedin, P. Steadman, A. Norris, R. McGrath, T. S. Turner, G. Thornton and N. M. Harrison, Phys. Rev. Lett. **86**, 3811 (2001).

[8] D. M. Duffy and J. H. Harding, Langmuir **20**, 7637 (2004).

[9] P. Hartman, Z. Kristallogr. **161**, 259 (1982).

[10] R. Kern, Bull. Soc. Fr. Mineral Cristallogr. **76**, 391 (1953); M. Bienfait, R. Boistelle, R. Kern, Adsorption et Croissance Cristalline. In *Colloques Internationaux du Centre National de la Recherche Scientifique*, Kern, R., Ed., Paris, France, 1965, Vol. 152, pp. 515-535.

[11] N. Radenović, W. van Enckevort, P. Verwer and E. Vlieg, Surf. Sci. **523**, 307 (2003); N. Radenović, W. van Enckevort, E and Vlieg, J. Cryst. Growth **263**, 544 (2004); N. Radenović, van W. Enckevort, D. Kaminski, M. Heijna and E. Vlieg, Surf. Sci. **599**, 196 (2005).

[12] A. Johnsen, Wachstum und Auflösung der Kristallen, Engelmann, Leipzig, 1910.

[13] F. Rohr, K. Wirth, J. Libuda, D. Cappus, M. Bäumer and H. J. Freund, Surf. Sci. **315**, L977 (1994); M. A. Langell, C. L. Berrie, M. H. Nassir and K. W. Wulser, Surf. Sci. **320**, 25 (1994).

[14] A. Wander, I. J. Bush and N. M. Harrison, Phys. Rev. B **68**, 233405 (2003).

[15] P. Hartman, Bull. Soc. franç. Minér. Crist. **LXXXII**, 158 (1959).

[16] R. Lacmann, Adsorption et Croissance Cristalline. In *Colloques Internationaux du Centre National de la Recherche Scientifique*, Kern, R., Ed., Paris, France, 1965, Vol. 152, pp. 195-214.

[17] D. Wolf, Phys. Rev. Lett. **68**, 3315 (1992).

[18] M. Bruno, D. Aquilano, L. Pastero and M. Prencipe, Crystal Growth & Design **8**, 2163 (2008).

[19] M. Bruno, D. Aquilano and M. Prencipe, Crystal Growth & Design **9**, 1912 (2009).

[20] R. Dovesi, V.R. Saunders, C. Roetti, R. Orlando, C. M. Zicovich-Wilson, F. Pascale, B. Civalleri, K. Doll, N.M. Harrison, I.J. Bush, Ph. D'Arco and M. Llunell, *CRYSTAL06 User's Manual*, University of Torino, Torino (2006).

[21] R. Dovesi, B. Civalleri, R. Orlando, C. Roetti and V.R. Saunders, in *Reviews in Computational Chemistry*, ed. B.K. Lipkowitz, R. Larter and T.R. Cundari, John Wiley and Sons Inc., New York, 2005, Vol. 21, pp. 1-125.

[22] W. M. M. Heijnen, N. Jb. Miner. Mh. **8**, 357 (1985).

[23] F. R. Massaro, L. Pastero, M. Rubbo and D. Aquilano, J. Cryst. Growth **310**, 706 (2008).

[24] M. Bruno, F. R. Massaro and M. Principe, Surf. Sci. **602**, 2774 (2008).

[25] A. L. Rohl, K. Wright and J. D. Gale, Am. Miner. **88**, 921 (2003).

[26] J. D. Gale, J. Chem. Soc. Faraday Trans. **93**, 629 (1997).

[27] M. Bruno, F. R. Massaro, M. Prencipe and D. Aquilano, Cryst.Eng.Comm. **12**, 3626 (2010).

[28] P. Curie, Journal de physique **3**, 393 (1894).